Analysis of fragments larger than 2 mm generated by a picosatellite fragmentation experiment

Lorenzo Olivieri [a,*], Cinzia Giacomuzzo [b], Alessandro Francesconi [b]

[a] *CISAS G, Colombo, Via Venezia 15, 35131, Padova, Italy*
[b] *Dipartimento di Ingegneria Industriale, Via Venezia 1, 35131, Padova, Italy*

A B S T R A C T

Satellite breakup models rely on laboratory tests and in-space collision observations; current models can match fragments distributions generated by traditional satellites but may need to be improved for small spacecraft and modern satellites employing new configurations and materials. In the last years, ground tests have been employed to assess the influence of dimensions, materials and internal configurations on fragments distributions and to define the limits of the current models. In this context, an impact test was performed at the impact facility of the University of Padova to characterize the fragmentation of a picosatellite mock-up; more than 7000 fragments were collected, classified and analysed with automatic image recognition algorithms. It was observed that the experimental characteristic length distribution is line with the prediction of the NASA SBM even for the smallest size classes, while the fragments shape distribution is strongly affected by the materials employed in the picosatellite manufacturing.

The subset of the collected fragments larger than 2 mm was recently subjected to a more detailed analysis: each fragment was individually weighed, and its three main dimensions were measured. In this paper, resulting fragments distributions are compared with literature data and the NASA Standard Breakup Model; in particular, an analytic relation between fragments characteristic length and size is found. In addition, results show that characteristic length and area-to-mass distributions are affected by the target materials and are clearly influenced by the size resolution of the analysed fragments.

1. Introduction

To date, the most employed set of equations used to evaluate spacecraft fragmentations in case of in-space collisions or explosions is the NASA Standard Breakup Model (SBM) [1]. It includes empirical relationships to calculate the cumulative number of fragments generated by an event as function of their characteristic length and predicts their area-to-mass ratio and relative velocity. The NASA SBM employs the Energy to Mass Ratio (EMR) parameter, defined as the impactor energy over mass of the involved bodies, to discriminate the severity of a collision: above the threshold of 40 J/g, the event is considered catastrophic, leading to the complete fragmentation of the colliding objects. While the NASA SBM provides reliable fragments distributions for historical collision events, possible improvements are under evaluation regarding the representativeness of state-of-the-art satellite configurations [2], the accuracy in modelling distributions of fragments smaller than few mm [3], and the capability to discern between central and glancing impacts [4,5]. In this context, recent investigations aim to better understand the phenomena involved in spacecraft fragmentation and to identify the main parameters affecting satellites breakup, with the final goal of developing new breakup models or tuning existing simulation tools [6–8].

Ground fragmentation tests are among the sources employed in this investigation process; together with observations and simulations of fragmentations, they allow the scientific community to evaluate the evolution of the space debris environment and to develop and validate breakup models. Regarding tests reported in the literature, the SOCIT experiment was performed on a metallic satellite mock-up in 1995 and its outcomes were included in the NASA SBM [1,9]; twenty years later, the DebriSat campaign studied the fragmentation of a satellite with novel design solutions and with a large fraction of non-metallic parts [10]. In addition, dedicated tests focused on small satellites breakup, investigating the influence of parameters such as the impactor kinetic energy [11–13] and the materials and masses distributions inside the

spacecraft [14]. More recently, a 1.5U CubeSat model was subjected to hypervelocity impact testing to study on the consequences of a catastrophic collision involving a nanosatellite [15].

In this context, in 2021 the University of Padova performed an impact test on a 5 × 5x5 cm³ picosatellite mock-up with a Nylon cylindrical projectile (diameter and height both of 12 mm) that hit the centre of one face of the satellite at 0 deg at a velocity of 2.72 km/s [16]. The mock-up included plastic elements and consumable electronic boards to simulate the different materials employed in modern spacecraft; the mass fraction of different materials is about 25% metals, 20% plastics, and 55% of electronic components (as reference, on Debrisat the metals fraction was larger than 87% [17]). The impact EMR was of about 80 kJ/kg, well above the catastrophic threshold, and the collision led to the complete fragmentation of the target; more than 7000 fragments were collected, weighed, and divided in size classes. A dedicated automatic image recognition software was employed to measure fragments shapes in 2-D; characteristic length cumulative distributions and shape distribution histograms were obtained [16]. Results showed that the NASA SBM captures well the characteristic length distributions, while that fragments shape and area-to-mass are clearly affected by source materials.

Recently, the subset of the collected fragments larger than 2 mm was subjected to a more detailed analysis: each object was individually weighed, and its three main dimensions were measured. In this paper, the analysis of this subset is presented, and the resulting fragments distributions are compared with the NASA Standard Breakup Model and with literature data.

In the next section, an overview of the impact parameters is introduced and information on the collected fragments is provided. The analysis of characteristic length, shape, mass, and area-to-mass follows. Results confirm that the picosatellite materials strongly affects the distributions; compared to literature data, results are clearly influenced by the size resolution of the analysed fragments, i.e. to the size of the smallest detectable object.

2. Picosatellite impact test

The test mock-up was designed to include different materials and components; it consisted in a plastic structure of four beams and two internal plates, external aluminium plates, batteries, and general-purpose COTS electric and electronic components stacked in three different levels (Fig. 1, left); a more detailed description of the picosatellite is reported in Ref. [16].

The impact experiment was carried out at the CISAS Hypervelocity Impact Facility using a two-stage Light-Gas Gun (LGG), capable of accelerating projectiles up to 100 mg at a maximum speed of 5.5 km/s [18–21]. The mock-up was hanged on a C-shaped support structure (Fig. 1, centre) and inserted in a dedicated box with soft walls to collect the generated fragments; the box was then installed inside the LGG impact chamber (Fig. 1, right).

A nylon cylinder (diameter of 12 mm, height of 12 mm) was employed as projectile; its mass was 1.66 g. The test velocity was 2.72 km/s (above the speed of sound for the non-metallic components of the picosatellite), and the projectile impacted the centre of one face of the target at an angle of 0 deg with respect to the normal: the resulting EMR was 80.65 kJ/kg, well above the catastrophic threshold of 40 kJ/kg. These impact parameters represent the limit of the current LGG configuration in terms of projectile kinetic energy; it is planned to perform additional tests on similar targets, employing smaller and faster projectiles (up to the limits of our LGG), to assess how higher velocities (but lower EMRs) influence catastrophic fragmentation.

The fragments generated by the test were extracted from the collision box and collected for their characterization; more than 7000 fragments were collected, 2-D scanned, and analysed with automatic image recognition algorithms, with an accuracy of 0.17 mm; the resulting fragments distributions can be found in Ref. [16].

This paper focuses on the fragments in the three largest size classes (all objects larger than 2 mm) were individually weighed and their three dimensions were measured, for a total of 530 fragments individually handled. A selection of the fragments larger than 2 mm can be seen in Fig. 2.

3. Data analysis

In this section the analysis of collected data is introduced and characteristic length, shape, mass, and area-to-mass distributions are presented.

3.1. Characteristic length distributions

In this subsection, cumulative distributions in function of fragments characteristic length are discussed. The characteristic length L_c is calculated as the arithmetic mean of three orthogonal dimensions a (larger size), b (second larger size), and c (smaller size) of the object:

$$L_c = \frac{a + b + c}{3} \tag{1}$$

Fig. 3 (left) compares the experimental data with the NASA SBM; the two trends are consistent for characteristic length larger than 2 mm. Below this threshold value, only few additional fragments are present; they consist in the few objects with a and possibly b larger than 2 mm (therefore belonging to the >2 mm class) but a smaller value for the minor size c (leading to a characteristic length $L_c < 2$ mm). Fig. 3 (right) reports the same data broken down for different fragments materials. It is shown that the majority of the objects are made of plastics (418 debris, red asterisk), with 65 metal fragments (black plus marker) and 47 objects generated by the on-board electronics (green cross). The plastics trend is comparable with the cumulative one, with the same slope of the NASA SBM; similarly, the metallic objects present a scaled-down distribution, whose slope is comparable to the NASA SBM. On the contrary, electronics fragments show a different, less steep, slope.
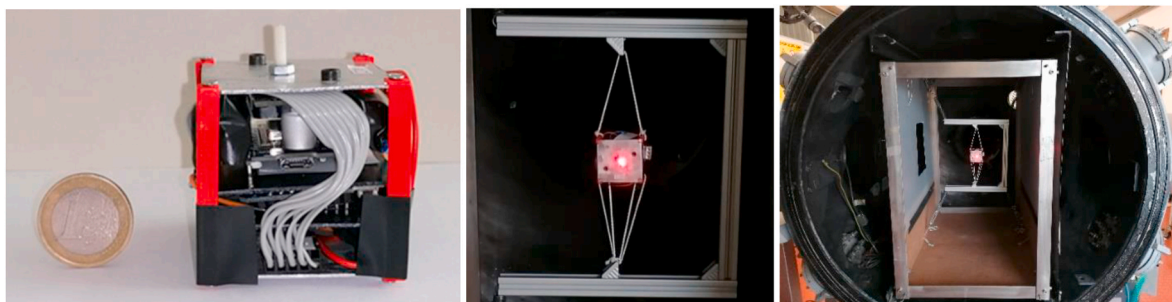

Fig. 1. Picosatellite layout (left) and test setup (centre and right). The red laser light spot is used for centring the picosatellite mock-up in the impact chamber. (For interpretation of the references to colour in this figure legend, the reader is referred to the Web version of this article.)
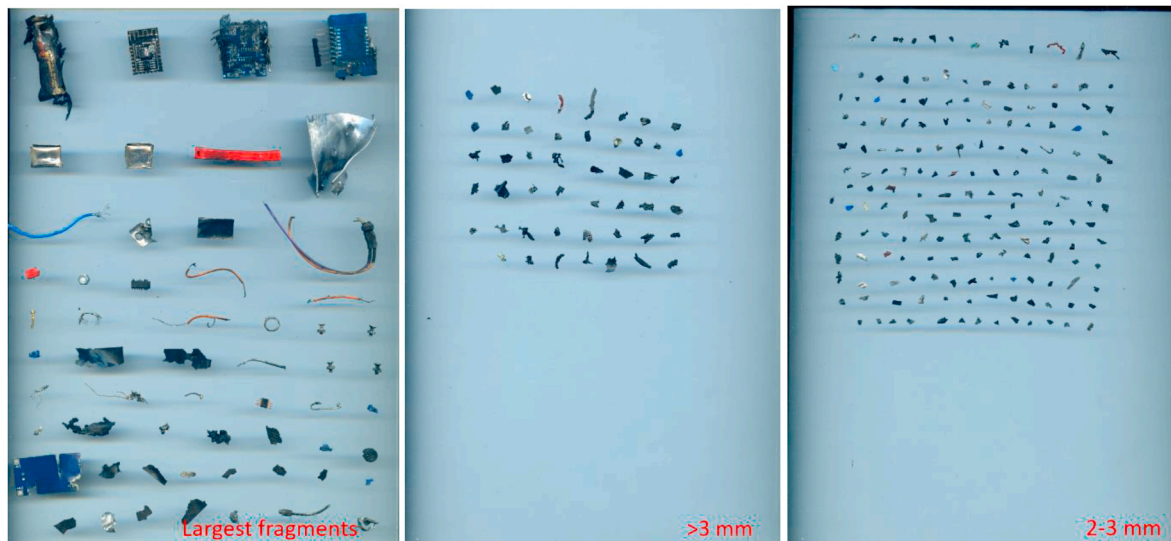
Fig. 2. A selection of the collected fragments divided for size classes. From left to right, largest fragments individually collected from the impact chamber, class larger than 3 mm, and class between 2 mm and 3 mm.
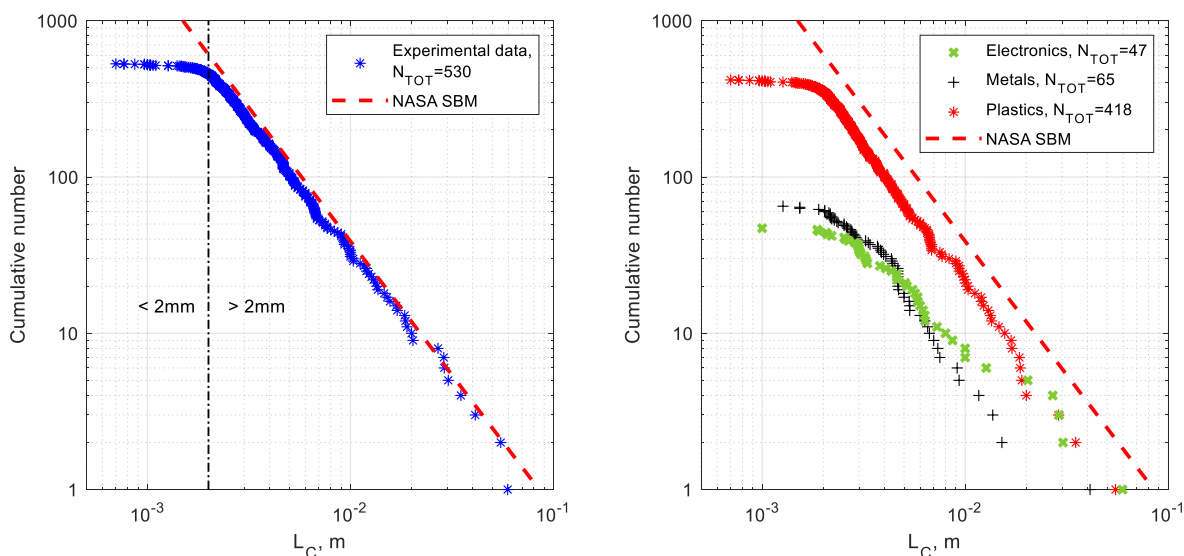

Fig. 3. Characteristic length cumulative distributions: on the left, comparison between experimental data and NASA SBM; on the right, distributions in function of fragments material.

3.2. Fragments shape

The shape of the fragments can be expressed as the ratio between its second larger on its larger dimensions (b/a) or as the ratio of the smaller on the larger size (c/a). Fig. 4 shows both ratios in terms of fragments material and characteristic length. It can be noted that the majority of the fragments presents a b/a ratio larger than 0.5 (i.e., the largest dimension is smaller than twice the second largest dimension); no direct dependence from the characteristic length or the material can be found. The c/a ratio is below 0.5 for most objects, again with no clear dependence from L_c or material. These results suggest that the majority of the generated fragments can be classified as "plates", i.e. objects with the two larger dimensions a and b significantly larger than the third one. Such results is compatible with the Picosatellite design: in a similar fashion to common spacecraft configuration, the mock-up consisted of stacked layers (the aluminium top and bottom faces, the internal plates, and the electronic boards), that were broken down in smaller planar sections by the impact.

3.3. Fragments mass

In this section the fragments mass distribution is presented. Fig. 5 (left) shows the mass in function of the characteristic length for all 530 fragments (blue markers); the average trend of this distribution can be modelled with least squares fit line (in the logarithmic space – solid line). In addition, the plot reports the L_c to mass distribution trend of the largest 100 fragments from the SOCIT experiment (dashed black line - [22,23]). It can be observed that there is a strong agreement between the two lines: the slope is the same (2.30) and the two intercepts are respectively 0.66 and 0.90; moreover, this trend is also in accordance with data from DebriSat [23]. The slight variation of the intercept can be related to the predominance of low-density fragments in the Picosatellite data. This is confirmed by the distributions broken down per material categories reported in Fig. 5 (right) and corroborates the effect of density on L_c-mass trends described by Hanada [24]. In fact, the majority of the plastic fragments (lower density, red asterisk) are below the metallic ones (higher density, black plus marker). Least square fits
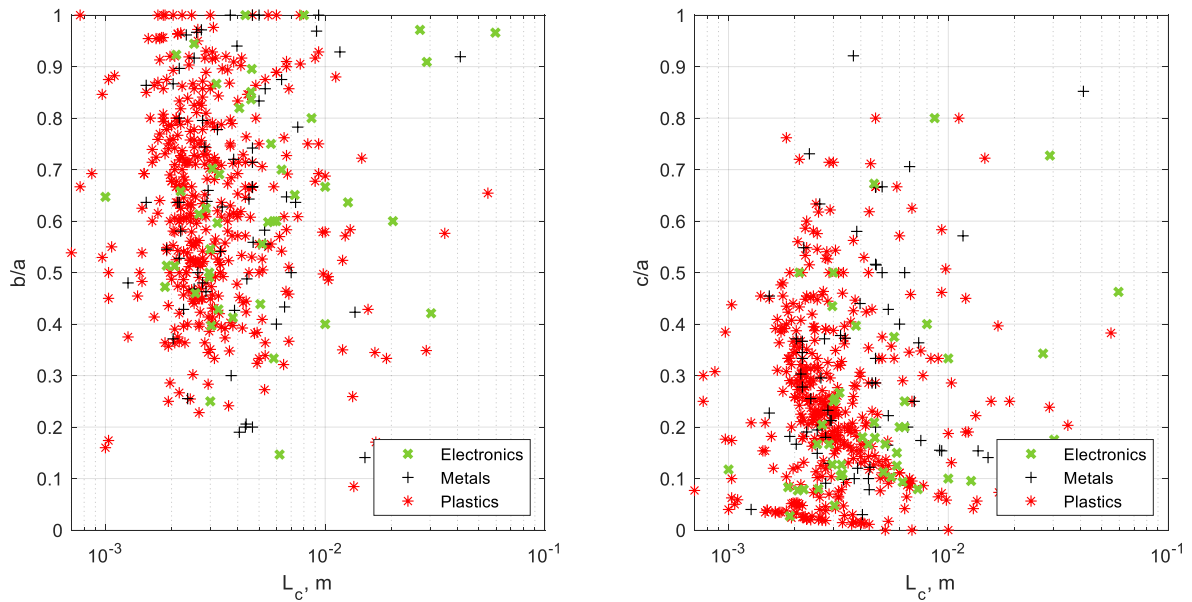
Fig. 4. Shape ratios in function of characteristic length and fragments material: on the left, *b/a*; on the right, *c/a*.
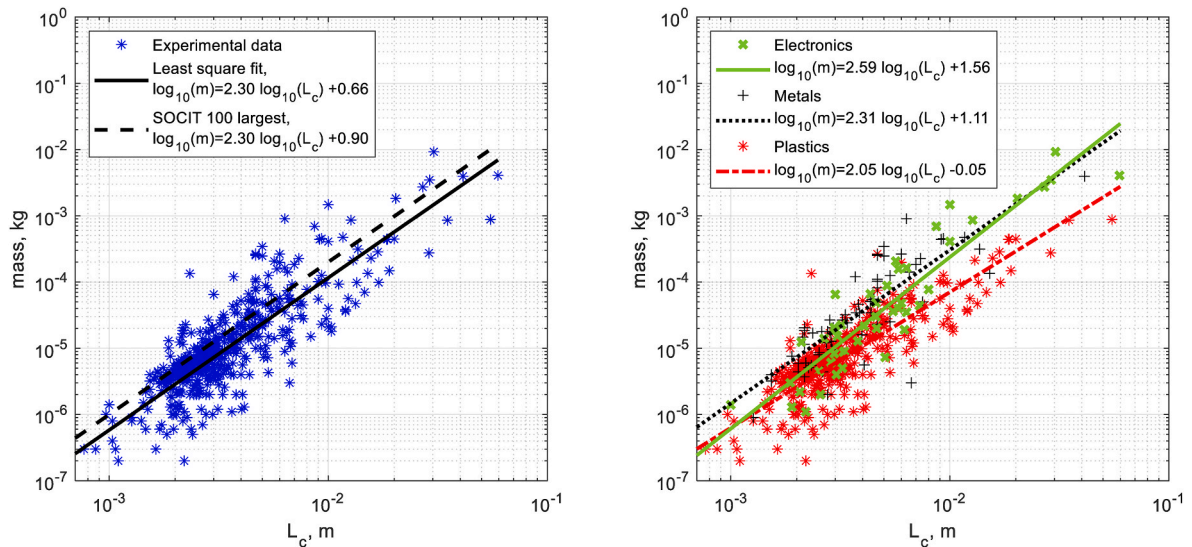

Fig. 5. Fragments mass in function of characteristic length. On the left, comparison of experimental data with the trend model (dashed line) from SOCIT 100 largest fragments; on the right, mass distribution broken down into material categories.

for each the material indicate that the metals distribution is on average very close to the SOCIT one, while the electronics one presents a larger angular coefficient (2.59) and the plastics distribution has a smaller one (2.05). It appears that for the selected data the electronics and the plastics distributions counterbalance each other, leading to an average trend comparable to the metals one.

On these considerations, it can be concluded that, for the considered data, the least squares fit of the L_c-mass distribution shows an angular coefficient of 2.30, regardless of the target design; the mock-up material density affects only the intercept. In the linear space, this relation becomes a power equation, as reported in Eq. (2):

$$m = 4.56 \, L_c^{-2.30} \tag{2}$$

3.4. Area to mass ratio

The area to mass is the ratio between the fragment cross-section and its mass. While the mass is directly measured, the area is derived from

the fragments characteristic length using the formulas from the NASA SBM model [1]:

$$A = 0.540424 \, L_c^2, \text{ where } L_C < 0.00167 \text{ m} \tag{3}$$

$$A = 0.556945 \, L_c^{2.047077}, \text{ where } L_C \geq 0.00167 \text{ m} \tag{4}$$

As reported in Ref. [16], the area-to-mass distribution is compared with the NASA SBM prediction (see Fig. 6, left). A substantial difference can be observed, with a translation of the distribution to higher values of the area-to-mass: the main peak is predicted at about −1.1 (0.08 m²/kg), while its real position is at about −0.25 (0.56 m²/kg). This translation was already observed in the literature and was attributed to the presence of lower density materials [13]. In fact, the dataset on which the NASA SBM is based derives from impact experiments and observations of breakup of satellites made of high-density materials; a large fraction of the picosatellite mock-up was composed by low density materials, determining the shift of the curve to higher area-to-mass ratios.
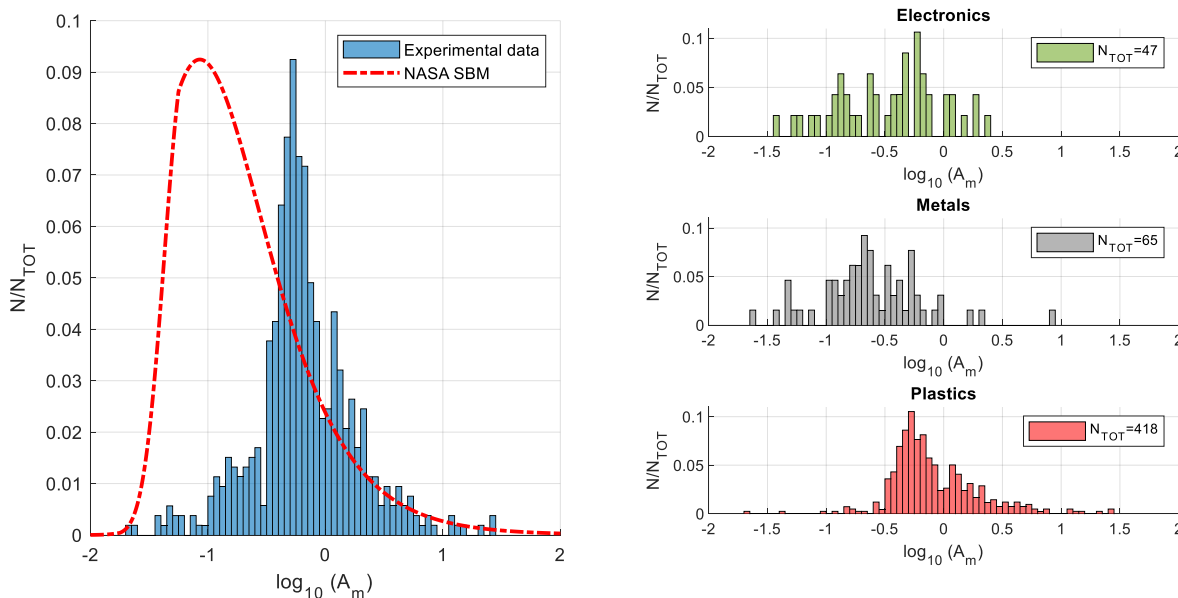
Fig. 6. Area-to-mass ratio distribution for fragments larger than 2 mm. On the left, comparison between experimental data (histogram) and NASA SBM prediction (red dashed line); on the right, from top to bottom, distributions for electronics, metals, and plastics fragments. (For interpretation of the references to colour in this figure legend, the reader is referred to the Web version of this article.)

The effect of the different materials can be appreciated in Fig. 6, right: plastic fragments present the same peak of the cumulative distribution and a similar trend for values on the x axis larger than −0.5 (0.32 m²/kg). For smaller area to mass ratios, the influence of metallic fragments is recognizable (main peak at about −0.7, 0.20 m²/kg). Last, the electronics debris distribution is more uniform in the range between −1.5 and 0.5 (between 0.03 m²/kg and 3.16 m²/kg), with its peak at −0.25 (0.56 m²/kg).

Fig. 7 (left) compares the area to mass ratio distributions in function

of the characteristic length of the experimental data and the observation of 1780 fragments generated from on-orbit breakup and employed in the development of the NASA SBM model [1]. It can be noted that the two distributions lie at different characteristic lengths: ground test data in the range from 0.7 mm to 5 cm, observations from 2 cm to more than 4 m. However, the main clusters of points are centred at about the same values of the area-to-mass ratio.

It shall be considered that both datasets present a resolution limit for the fragments size: ground test data was limited to objects >2 mm, while
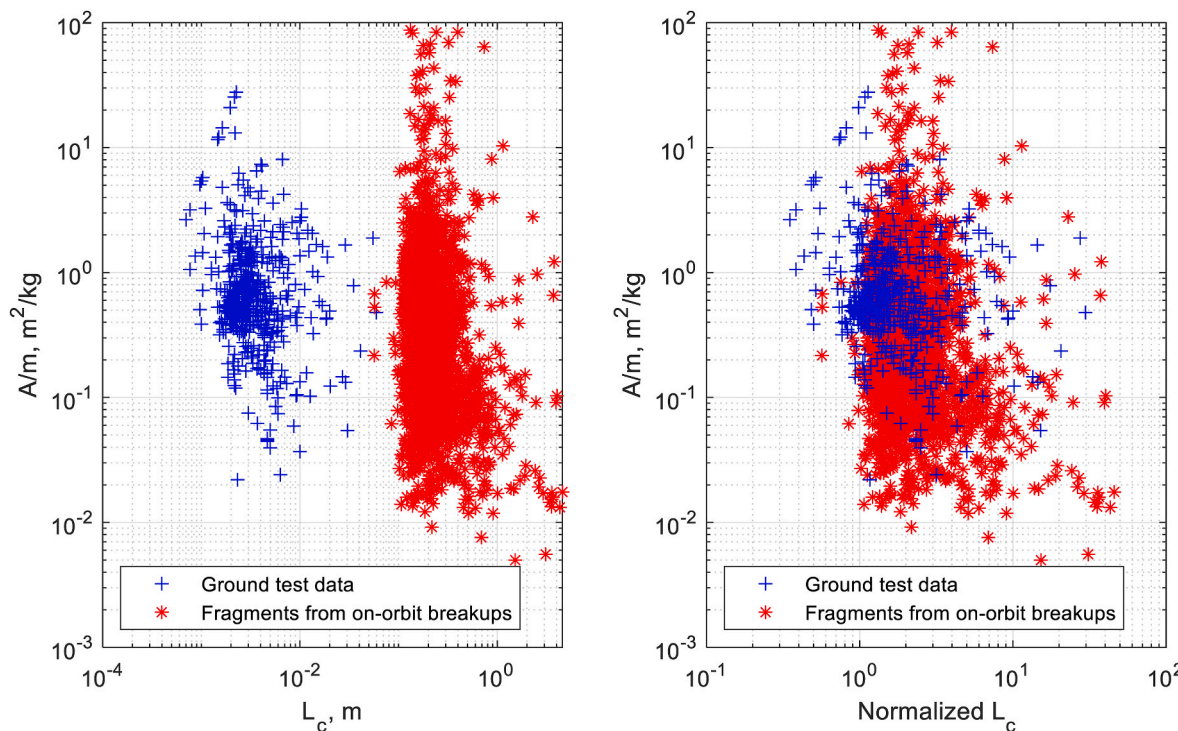

Fig. 7. Area-to-mass in function of characteristic length. On the left, comparison of experimental data (blue plus markers) and observations of 1780 fragments from on-orbit breakup (red asterisks) [1]; on the right, same data with the characteristic length normalized on fragments acquisition resolution size. (For interpretation of the references to colour in this figure legend, the reader is referred to the Web version of this article.)

the ground observations to debris >10 cm [1]. Fig. 7 (right) reports the same distributions with the characteristic length normalized on these resolution values (2 mm for ground test, 10 cm for observations): it can be noted that the two main clusters are overlapping. A few fragments from the picosatellite present x-axis values below 1 (their characteristic length is lower than the collection resolution); this is consistent with the observations on fragments shape, as the majority of the generated fragments can be classified as "plates" (objects with the two larger dimensions *a* and *b* consistently larger than the third one), with a characteristic length smaller than their larger dimension. With respect to the area-to-mass, the observation data cluster shows a consistent fraction of objects below $0.3\,m^2/kg$ (lower limit of ground test data cluster). In fact, this is consistent with the previous conclusions: the presence of low-density materials in the picosatellite generates a translation of the area-to-mass distribution to higher values.

4. Discussion

In the previous sections, it was observed that the L_c-mass distribution of the ground test data is consistent with the trend from SOCIT 100 largest fragments. By contrast, the NASA SBM area-to-mass model, despite being developed with the contribution of SOCIT data and a function of both the mass and the characteristic length, does not represent the picosatellite fragments distribution.

It shall be underlined that, for the L_c-mass distribution, the least squares fit indicates an "average" value of the mass for each characteristic length; however, it does not provide any information on the number of the fragments that may generate this distribution. As reference, the same least squares fit could represent a distribution with few small and light fragments and a lot of large and heavy objects, as well as one with a larger number of small and light fragment and less large and heavy objects.

Eq. (2) (power law relating fragments characteristic length and mass) and Eqs. (3) and (4) (fragments cross section in function of their characteristic length, from NASA SBM) suggests that, on average, the area to mass can be directly expressed in terms of characteristic length. It shall be underlined that Eqs. (3) and (4) have two different formulations for L_c below and above a threshold of 1.67 mm; for the range of characteristics lengths considered in this work (up to about 5 cm for the picosatellite fragments) the difference between the two formulation is always below 2%; Eq. (3) is therefore considered representative for the whole experimental dataset. On these considerations, it is possible to calculate the average area-to-mass by merging Eqs. (2) and (3):

$$A\,/\,m = 0.12\,L_c^{-0.30} \tag{5}$$

Fig. 8 compares ground test data (divided for materials) with the power models reported in Eq. (2) and Eq. (5). The mass distribution (left) is on average well represented by the relative model, with a co-efficient of determination R^2 of 0.69. With respect to the area-to-mass, experimental data is extremely scattered; in this case the coefficient of determination is 0.03. In fact, while Eq. (5) might be representative of the average value of the area-to-mass, it does not provide information on the extremely high variance of this parameter.

On the other hand, area-to-mass histograms (see Fig. 6) show the fraction of fragments whose area-to-mass lie in a certain range; therefore, they provide a quantitative information on the fragments number per class. In fact, different fragment distributions may have the same least squares fit for the area-to-mass but generate different histograms. For this reason, an agreement on the L_c-mass trend and the existence of a simplified model of the area-to-mass in function of the characteristic length do not directly implicate the accordance of area-to-mass histograms to the NASA SBM model.

5. Summary and conclusions

This paper presented the analysis of 530 fragments larger than 2 mm generated by the impact test on a picosatellite. All fragments were measured and weighed, and characteristic length, shape, mass, and area-to-mass distributions were generated.

For characteristic length, the comparison with the NASA SBM confirmed that the model is representative of the experimental data: for a target without appendages the characteristic length distribution maintains the predicted slope. Fragments shape analysis suggest that the majority of the generated fragments can be classified as "plates", objects with the two larger dimensions *a* and *b* consistently larger than the third one. This is consistent with the Picosatellite design and the internal configuration of many modern satellites: a large fraction of the components consists in thin plates (aluminium top and bottom faces, internal plates, electronic boards), that fragmented in smaller sections. The analysis of fragments mass in function of their characteristic length suggests a consistent agreement with trends derived from the SOCIT experiment data. In both cases, the least squares fit of the characteristic length – mass distribution shows an angular coefficient of 2.30, regardless of the target design; the objects materials affect only the
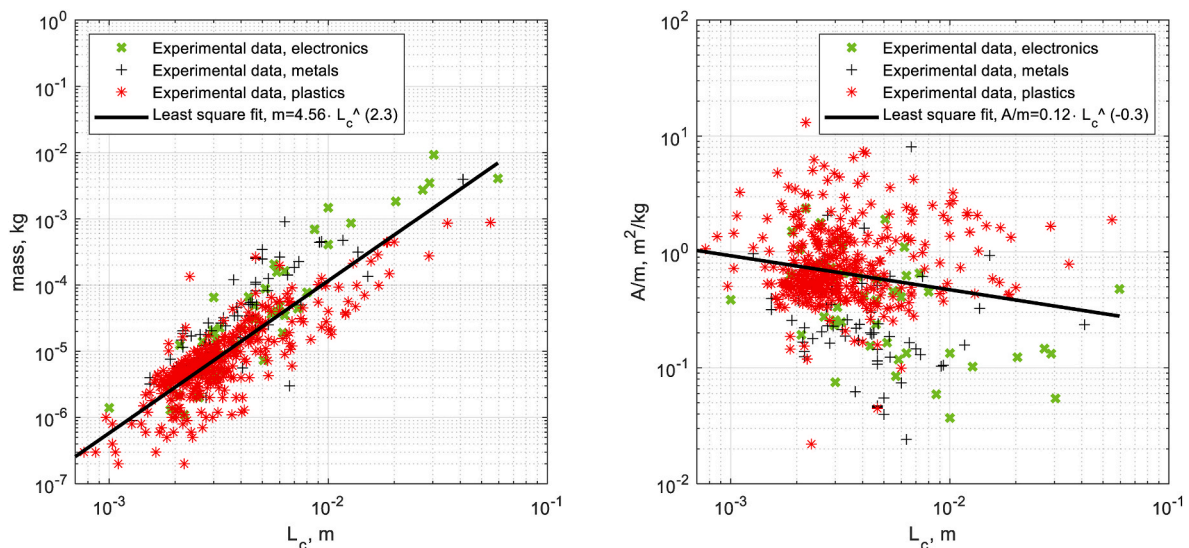

Fig. 8. Mass (left) and area-to-mass (right) in function of characteristic length: comparison between experimental data (coloured markers) and least squares fit model (solid black line).

intercept. Area-to-mass ratio distribution for the fragments larger than 2 mm are not well represented by the NASA SBM: the low-density materials employed in the mock-up influence the shape and the values of the distribution, which is translated to higher values of the area-to-mass with respect to the NASA model. Last, a power relationship between the characteristic length and the area to mass is derived; while this model can provide information "on average", it cannot be employed to define area-to-mass distribution histograms.

In conclusion, data presented in this work suggest that for the considered impact configuration there is a good agreement among experimental data, observations, and models both for characteristic length and mass distributions; the power model relating these two parameters presents a coefficient of determination $R^2 = 0.69$. By contrast, the area-to-mass distributions are affected by materials choice and the derivation of a model is limited to average values; in this case, the prediction from the NASA SBM is less accurate.

In the future, it will be important to assess the influence of spacecraft materials on the debris generation and to develop models capable to include their effect. It is recommended to perform additional ground tests, both at component and system levels, to investigate the break-up process and update the current fragmentation models.

Declaration of competing interest

The authors declare that they have no known competing financial interests or personal relationships that could have appeared to influence the work reported in this paper.

Acknowledgments

References

[1] N.L. Johnson, P.H. Krisko, J.C. Liou, P.D. Anz-Meador, NASA's new breakup model of EVOLVE 4.0, Adv. Space Res. 28 (9) (2001) 1377–1384.

[2] Si-yuan Ren, et al., Satellite Breakup Behaviors and Model under the Hypervelocity Impact and Explosion: A Review, Defence Technology, 2022.

[3] Alessandro Francesconi, et al., Numerical simulations of hypervelocity collisions scenarios against a large satellite, Int. J. Impact Eng. 162 (2022), 104130.

[4] M. Schimmerohn, P. Matura, E. Watson, N. Durr, A. Altes, T. Cardone, F. Schäfer, Numerical investigation on the standard catastrophic breakup criteria, Acta Astronaut. 178 (2021) 265–271.

[5] L. Olivieri, et al., Investigation of ENVISAT catastrophic fragmentation scenarios, 72nd International Astronautical Congress (IAC (2021) 2021.

[6] Nicola Cimmino, et al., Tuning of NASA standard breakup model for fragmentation events modelling, Aerospace 8 (2021) 185.

[7] Alessandro Francesconi, et al., CST: a new semi-empirical tool for simulating spacecraft collisions in orbit, Acta Astronaut. 160 (2019) 195–205.

[8] Lorenzo Olivieri, et al., Simulations of satellites mock-up fragmentation, IAC (2022) 18–22. September 2022.

[9] D. McNight, N. Johnson, M. Fudge, T. Maclay, Satellite Orbital Debris Characterization Impact Test (SOCIT), Kaman Sciences Corporation, Colorado Springs, CO, 1995.

[10] J.C. Liou, N. Fitz-Coy, S. Clark, M. Werremeyer, T. Huynh, M. Sorge, J. Opiela, DebriSat–A planned laboratory-based satellite impact experiment for breakup fragment characterization, in: Sixth European Conference on *Space Debris*, ESA Communications, 2013, August.

[11] T. Hanada, et al., Micro-satellite Impact Testing", *27th International Symposium On Space Technology And Science*, 2009. Tsukuba, Japan, 2009.

[12] T. Hanada, J.-C. Liou, Comparison of fragments created by low-and hyper-velocity impacts, Adv. Space Res. 41 (2008) 1132–1137.

[13] K. Sakuraba, Y. Tsuruda, T. Hanada, J.C. Liou, Y. Akahoshi, Investigation and comparison between new satellite impact test results and NASA standard breakup model, Int. J. Impact Eng. 35 (12) (2008) 1567–1572.

[14] S.W. Lan, S. Liu, Y. Li, F.W. Ke, J. Huang, Debris area distribution of spacecraft under hypervelocity impact, Acta Astronaut. 105 (1) (2014) 75–81.

[15] H. Abdulhamid, D. Bouat, A. Collé, J. Lafite, J. Limido, I. Midani, P. Omaly, On-ground HVI on a nanosatellite. Impact test, fragments recovery and characterization, impact simulations, 8th European Conference on Space Debris (2021).

[16] Lorenzo Olivieri, et al., Characterization of the fragments generated by a Picosatellite impact experiment, Int. J. Impact Eng. 168 (2022), 104313.

[17] Rafael E. Carrasquilla, Fitz-Coy Norman, DebriSat: generating a dataset to improve space debris models from a laboratory hypervelocity experiment, Europe 361 (2019) 5–638.

[18] F. Angrilli, D. Pavarin, M. De Cecco, A. Francesconi, Impact facility based upon high frequency two stage light-gas gun, Acta Astronaut. 53 (3) (2003) 185–189, https://doi.org/10.1016/S0094-5765(02)00207-2.

[19] D. Pavarin, A. Francesconi, Improvement of the CISAS high-shot frequency light-gas gun, Int. J. Impact Eng. 29 (1–10) (2004) 549–562, https://doi.org/10.1016/j. ijimpeng.2003.10.004.

[20] D. Pavarin Francesconi, A. Bettella, F. Angrilli, A special design condition to increase the performance of two-stage light-gas guns, Int. J. Impact Eng. 35 (Issue 12) (December 2008) 1510–1515, https://doi.org/10.1016/j. ijimpeng.2008.07.035.

[21] A. Francesconi, et al., A special design condition to increase the performance of two-stage light-gas guns, Int. J. Impact Eng. 35 (2008) 1510–1515.

[22] P.H. Krisko, M. Horstman, M.L. Fudge, SOCIT4 collisional-breakup test data analysis: with shape and materials characterization, Adv. Space Res. 41 (2008) 1138–1146.

[23] J. Murray, H. Cowardin, J.C. Liou, M. Sorge, N. Fitz-Coy, T. Huynh, Analysis of the DebriSat fragments and comparison to the NASA standard satellite breakup model, in: International Orbital Debris C*onference (IOC (No*, JSC-E-DAA-TN73918, 2019, December.

[24] Toshiya Hanada, et al., Outcome of recent satellite impact experiments, Adv. Space Res. 44 (2009) 558–567.